AIDA-PUB-2011-018

AIDA

Advanced European Infrastructures for Detectors at Accelerators

Journal Publication

Simulations of planar pixel sensors for the ATLAS high luminosity upgrade

Calderini, G (Laboratoire de Physique Nucleaire et des Hautes Energies, Università degli Studi di Pisa/Istituto Nazionale di Fisica Nucleare) *et al*

21 April 2011

The research leading to these results has received funding from the European Commission under the FP7 Research Infrastructures project AIDA, grant agreement no. 262025.

This work is part of AIDA Work Package **9: Advanced infrastructures for detector R&D**.

The electronic version of this AIDA Publication is available via the AIDA web site <http://cern.ch/aida> or on the CERN Document Server at the following URL: <http://cds.cern.ch/search?p=AIDA-PUB-2011-018>

Nuclear Instruments and Methods in Physics Research A 636 (2011) S37–S41

Contents lists available at ScienceDirect

Nuclear Instruments and Methods in Physics Research A

journal homepage: www.elsevier.com/locate/nima

Simulations of planar pixel sensors for the ATLAS high luminosity upgrade

G. Calderini [a,b,*], M. Benoit [c], N. Dinu [c], A. Lounis [c], G. Marchiori [a]

[a] Laboratoire de Physique Nucléaire et des Hautes Énergies, Paris VI CNRS, Paris, France
[b] Università degli Studi di Pisa/Istituto Nazionale di Fisica Nucleare, sez. di Pisa, France
[c] Laboratoire de l'accèlèrateur linèaire, Orsay, France

ARTICLE INFO

Available online 29 April 2010

Keywords:
Silicon detectors
Pixel detectors
Tracking
Radiation damage

ABSTRACT

A physics-based device simulation was used to study the charge carrier distribution and the electric field configuration inside simplified two-dimensional models for pixel layouts based on the ATLAS pixel sensor. In order to study the behavior of such detectors under different levels of irradiation, a three-level defect model was implemented into the simulation. Using these models, the number of guard rings, the dead edge width and the detector thickness were modified to investigate their influence on the detector depletion at the edge and on its internal electric field distribution in order to optimize the layout parameters. Simulations indicate that the number of guard rings can be reduced by a few hundred microns with respect to the layout used for the present ATLAS sensors, with a corresponding extension of the active area of the sensors. A study of the inter-pixel capacitance and of the capacitance between the implants and the high-voltage contact as a function of several parameters affecting the geometry and the doping level of the implants was also carried out. The results are needed in order to evaluate the noise and the cross-talk among neighboring pixels when connected to the front-end electronics.

1. Introduction

The LHC is planning to increase its design luminosity from 10^{34} to $1–1.5\times10^{35}\,cm^{-2}\,s^{-1}$ through an upgrade program that should be completed by 2018 [1]. This increase in luminosity will have two main consequences for the ATLAS Inner Tracker. The radiation damage to the sensors and the electronics will be much higher with respect to the first phase of the LHC. The addition of a B-layer at a reduced distance from the interaction point (37 mm instead of the present 50 mm) will make this point even more critical. An equivalent 1 MeV neutron fluence of $10^{16}\,n_{eq}\,cm^{-2}$ is foreseen at that radius, a factor 10 higher than the fluence expected for the present detector.

A second consequence of the luminosity upgrade will be the rise in the detector occupancy. A reduced pixel size will probably be necessary and the tracking capability could benefit from the reduction of the detector thickness and improved sensor layout. In addition to the planar pixel technology, also other solutions are being investigated, such as 3D sensors [2] and diamond sensors [3]. Even for the standard planar pixel technology, the HEP community will need to re-design the detector in view of the challenges linked to the high luminosity, taking advantage of the evolution in electronics and semiconductor industry which took place in the last ten years.

2. The sensor simulation

In this paper we present a simulation developed to study the electrical features of different layouts of planar pixel sensors, in view of the construction of the ATLAS Insertable B-Layer (IBL) and the SLHC upgrade. The main goal is to optimize the sensor layout and to improve the tracking performance. The role of the simulation in this process has many aspects. Among others, the limited space available for the IBL and the general need to go as close as possible to the interaction point will make sensor shingling unpractical: the active area of the sensor has to be maximized, through a careful study of the guard ring and edge region; the detector thickness must be reduced to improve the material budget, favoring the full depletion of the sensor at high dose. The device thinning requires a precise evaluation of sensor properties, such as pixel capacitance; the radiation damage at different stages of the detector lifetime will influence the depletion voltage, changing under certain conditions the detector capability to collect charge. All these effects need to be studied with the simulation. At the same time, in parallel with the simulation process, a prototype submission has been commissioned to a few foundries [4]. Measurements on the produced sensors and test structures will allow to refine the parameters

* Corresponding author.
E-mail address: giovanni.calderini@cern.ch (G. Calderini).

0168-9002/$ - see front matter © 2010 Elsevier B.V. All rights reserved.
doi:10.1016/j.nima.2010.04.082

used in the simulation through an iterative process. The option considered in the simulation for the sensor production are both the n-in-n technology, similar to the one used in the present ATLAS detector, and n-in-p devices. For each hypothesis, variations in the number of guard rings and guard ring configurations (position, spacing, distribution) have been simulated. Different detector thickness values have been investigated. The effect of radiation damage has been introduced and different dose scenarios have been considered.

3. The simulation software

We used the Silvaco TCAD simulation software framework [5], produced by Silvaco International INC. In the framework of this application, the devices can be built with two alternative approaches. The fabrication process can be simulated if the fabrication parameters (implantation energies, doses, diffusion temperature and duration, oxidation) are known in detail. If this is not possible, the devices can be built directly through definition of regions and their properties (doping, implant sizes, depths, profiles etc). Both approaches have been used in this work.

The simulation solves the Poisson equation and the continuity equation on a lattice inside the device, taking into account the charge distribution from impurity ionization, the trap-levels in the bandgap (Shockley–Read–Hall generation recombination model [6]) the charges released from impact ionization (Crowell–Sze model [7]).

The behavior of the detector after irradiation is simulated through a model of the defect energy state distribution. This allows to extract the depletion voltage [8], the double peak in the electric field and the space charge sign inversion for n-bulk detectors [9–11]. A surface charge layer has been introduced in the irradiation scenarios to simulate surface damage to the oxide-silicon boundary.

4. The device geometry

At this stage, we used a simplified 2D model for the detector (see Fig. 1). We considered an half-infinite geometry in x and y, thus assuming that the effects we are studying are not influenced by the finite size of the device in these directions. A specific model has been used to reproduce the electrical properties of the edge cut, which acts as a conductive channel in the presence of a potential difference. The border region has been built as amorphous Silicon, with a gradual transition towards the crystal structure over a span of about 20 μm. A continuum of levels has been introduced in the bandgap [12]. The detector thickness is 300 μm. The guard ring configuration is critical to control the drop of potential at the edge of the detector and to protect against breakdown. It determines the active area of the detector, by granting an undepleted region (even if as thin as possible) at the edge. The behavior of the structure is influenced not only by process parameters but also by radiation damage. For this reason, an optimization of the layout needs to be made considering the different phases of the detector lifetime.

5. The n-in-p devices

The simulated n-in-p sensors are built starting from a 2 kΩ cm high resistivity substrate. N^+ implantation doses in the range (10^{13}–10^{16} cm^{-2}) at an energy of 120 keV have been investigated. The isolation is achieved by p-spray implants, with doses in the range (10^{11}–10^{13} cm^{-2}) at 115 keV. Different guard rings layouts have been studied, corresponding to real device submissions. A first option, called model A, presents nine guard rings with a variable spacing over a region of 603 μm (see Fig. 2) and a 500 μm edge region between the cut and the outermost guard ring, not included in the plot.

A second design, called model B, is based on a structure of 17 guard ring equally spaced over a region of 547 μm, with an edge of 311 μm. Finally a last option, model C, is based on 16 guard rings with two different pitch values over a region of 775 μm, and a 500 μm edge area.

Breakdown potential and the presence of breakdown locations have been studied for the different designs, together with the voltage distribution across the guard ring region and the behavior of the edge. A summary of the simulated breakdown voltages of

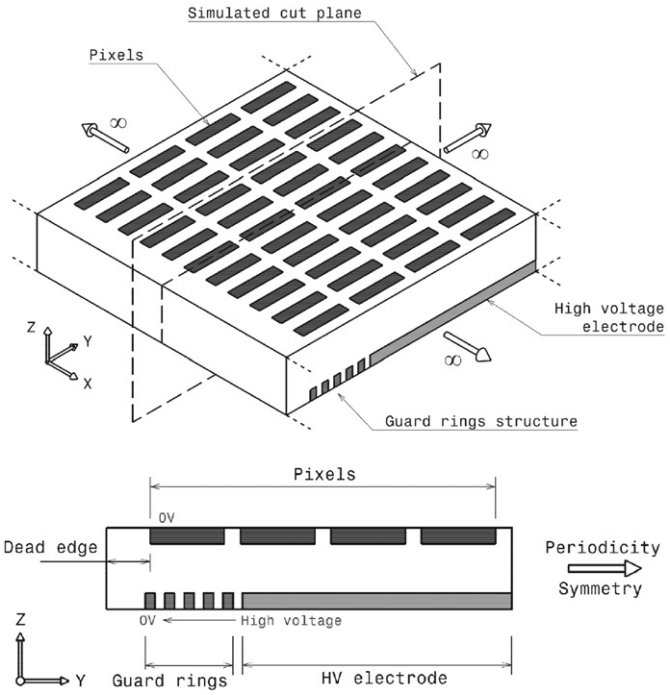

Fig. 1. Example of the half-infinite geometry with reference axes. In this picture the configuration for n-in-n sensors is shown: 3D view of the sensor (top) and YZ cross-section (bottom). The same pixel orientation is used for n-in-p devices.

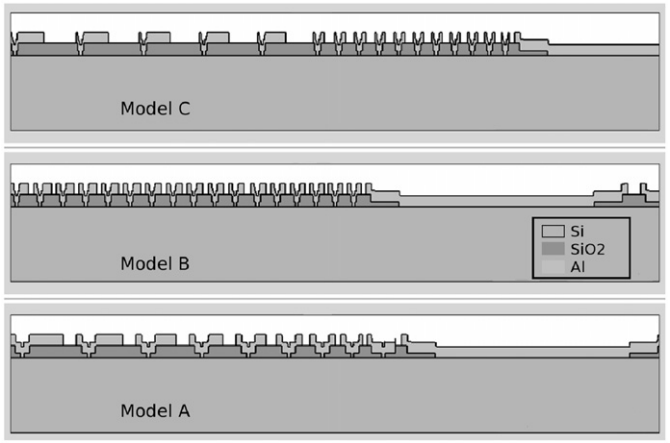

Fig. 2. Different layouts for the n-in-p simulated devices, addressed as C, B and A in the text. The edge regions, between the cut and the outermost guard ring, lie on the left of the picture and are not included in the plot.

unirradiated sensors as a function of the pixel and p-spray implantation doses is given for the model A, B and C devices in Tables 1–3.

The effect of radiation damage is then introduced and the study repeated. A three-level model, as described in Ref. [13] is used. The effect of oxide charge is simulated by adding a layer of charge ($2\times10^{12}\,cm^{-2}$) in the Silicon–oxide interface. The default value of oxide charge density for un-irradiated sensors was $10^{11}\,cm^{-2}$. Even if the submitted detectors and test structures are not yet available, we tested the reliability of this model by using measurements made on existing n-in-p structures before and after a $5\times10^{15}\,n_{eq}\,cm^{-2}$ irradiation. The potential distribution across the guard ring region for the real devices and the simulation is presented in Fig. 3. The agreement, even if not perfect is still remarkable, considering the rather high dose.

The breakdown voltages for n-in-p devices of model A, with a $3.16\times10^{12}\,cm^{-2}$ p-spray implantation dose, after a simulated fluence of $10^{15}\,n_{eq}\,cm^{-2}$ are given as example in Table 4 as a function of the initial implant concentrations.

The baseline of the study for the n-in-p devices is that all the models have a wide range of the parameters for which the breakdown voltage results of the order of 600 V or larger, thus preventing discharge effects, and the edge insulation is good. It has to be noted indeed that in the heavy irradiation scenarios ($n_{eq}>10^{15}\,cm^{-2}$) the detectors are not fully depleted anymore at 600 V, thus the charge collection is only partial. Nevertheless the detector can still be efficiently operated under these conditions, as other studies have shown, see for example Refs. [14,15].

6. The n-in-n devices

The simulated n-in-n sensors are built using a $10^{12}\,cm^{-3}$ n-doped substrate with $10^{18}\,cm^{-3}$ doped implants presenting a Gaussian profile in depth (1 μm). The layout configuration is similar to the C model for n-in-p devices and sets of 16, 15, 13 and 12 guard rings are used. The potential drop distribution in the guard ring region has been analyzed for the different configurations as shown in Fig. 4. The study has been then repeated for different radiation doses. In Fig. 5, the voltage distributions at 600 V are presented for the 16 guard ring sensor layout and fluences going from 0 to $10^{15}\,n_{eq}\,cm^{-2}$. The plot indicates that the drop of potential across the guard ring region becomes less uniform with the dose and the innermost guard rings tend to be

Table 1
Breakdown voltages as a function of the simulated implant and p-spray concentrations for model A detectors.

n^+ implantation dose (cm^{-2})	Model A p-spray implantation dose (cm^{-2})		
	3.16e12	3.5e12	1e13
1.00e+14	590 (V)	412	95
4.64e+14	625	519	139
2.15e+15	580	484	123
5.00e+15		473	
1.00e+16	565	443	122

Table 2
Breakdown voltages as a function of the simulated implant and p-spray concentrations for model B detectors.

n^+ implantation dose (cm^{-2})	Model B p-spray implantation dose (cm^{-2})			
	1e11	4.6e11	2.15e12	1e13
1.00e+14	> 600 (V)	> 600	560	90
4.64e+14	> 600	> 600	576	87
2.15e+15	> 600	> 600	> 600	100
5.00e+15	> 600	596	550	116
1.00e+16	> 600	575	> 600	210

Table 3
Breakdown voltages as a function of the simulated implant and p-spray concentrations for model C detectors.

n^+ implantation dose (cm^{-2})	Model C p-spray implantation dose (cm^{-2})			
	1e11	4.6e11	4.64e12	1e13
1.00e+14	> 600 (V)	> 600	179	80
4.64e+14	> 600	> 600	214	96
2.15e+15	> 600	> 600	250	122
5.00e+15	> 600	> 600	304	141
1.00e+16	> 600	> 600	373	130

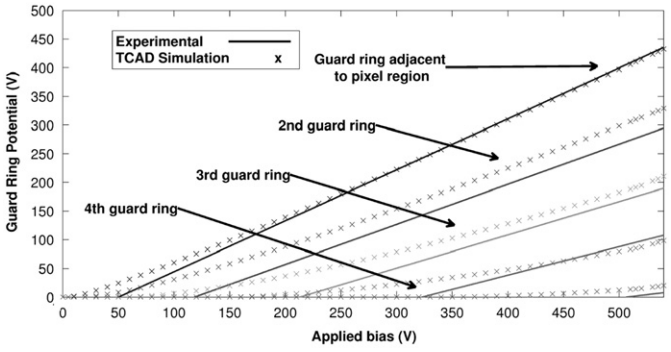

Fig. 3. Comparison between simulated and measured voltage of guard rings as a function of the bias voltage for n-in-p test devices irradiated at $5\times10^{15}\,n_{eq}\,cm^{-2}$. The guard ring numbering convention starts from 1 for the innermost guard ring and increases for outer guard rings with their distance from the pixel.

Table 4
Simulated breakdown voltages after $10^{15}\,n_{eq}\,cm^{-2}$ irradiation as a function of the initial n^+ implantation dose for model A detectors.

Model A				
n^+ implantation dose (cm^{-2})	1e14	4.64e14	2.15e15	1e16
Breakdown (V)	556	605	542	512

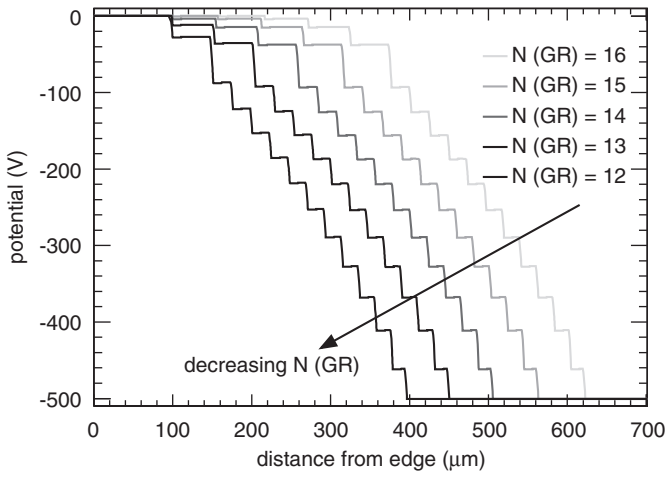

Fig. 4. Voltage distribution across the guard ring region for sensors with 12, 13, 14, 15 and 16 guard rings.

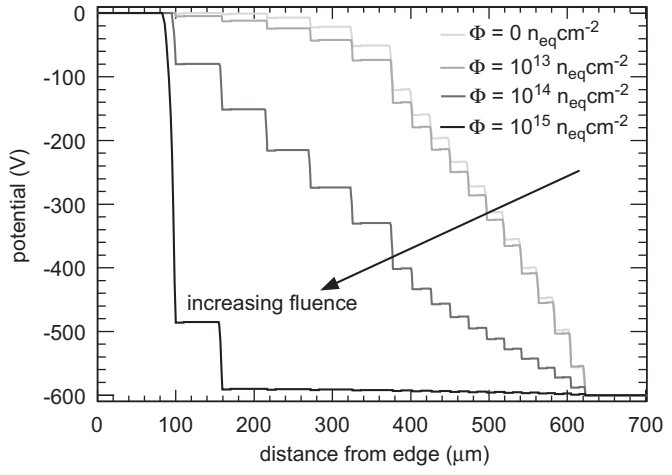

Fig. 5. Voltage distribution across the guard ring region for different fluences: 0, 10^{13}, 10^{14}, $10^{15}\,n_{eq}\,cm^{-2}$.

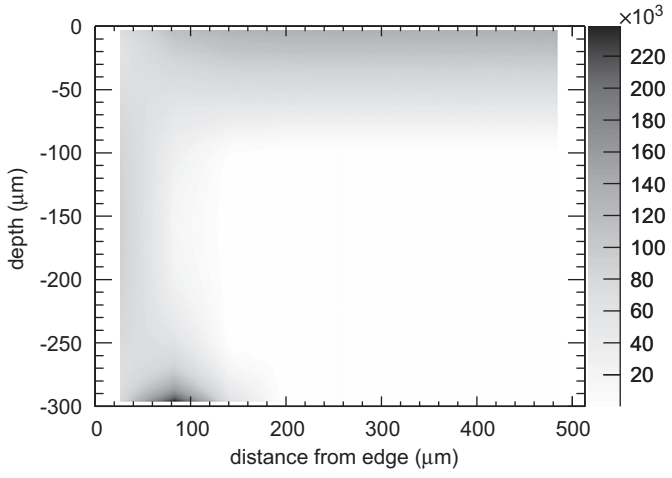

Fig. 6. Electric field distribution (V/cm) inside a n-in-n detector with 16 guard rings after a fluence of $10^{15}\,n_{eq}\,cm^{-2}$.

less efficient. In particular the electrical field distribution inside the sensor has been simulated at different doses to study the presence of points of breakdown or high current and to analyze the distance of the depleted region from the edge. As in the case of the n-in-p sensors, there is indication that the breakdown is still manageable to about 600 V, even if at fluences larger than $10^{15}\,n_{eq}\,cm^{-2}$ the detectors are not fully depleted anymore (see Fig. 6).

7. Thinning and pixel capacitance

Reducing the sensor thickness can be very important to maintain a reasonable material budget, in order to reduce multiple scattering and preserve the tracking performance. On the other hand, the signal collected with thinned sensors is smaller than for thicker ones. This plays a role in the optimization of the readout electronics. Capacitance evaluation for different thickness hypothesis is needed in order to extrapolate the detector performance in terms of noise and charge sharing. For this reason, the pixel capacitance has been studied in the simulations for different thickness options. The size of the pixels has been considered to be $50 \times 400\,\mu m^2$ (for direct comparison with the present detector) and $50 \times 250\,\mu m^2$. The same baseline parameters used in the simulation of the n-in-n devices have been used. Since we used a 2D simulation, the capacitance towards the neighbours has been obtained by calculating a "per-unit-length capacitance" with structures 1-μm−wide along the side facing the corresponding neighbours. The contribution to the total capacitance has then been computed by multiplying this value for the actual pixel width in this direction. Presently only unirradiated sensors have been simulated.

The main result of the capacitance study is that in the considered configurations the most important contribution is given by the capacitance towards the first neighbour pixels. The capacitance towards the second neighbours is negligible, as well as the capacitance towards the backplane. The total capacitance is of the order of 100 fF. Fig. 7 shows the capacitance dependence on the sensor thickness, the pixel size, the pixel doping and the p-spray doping concentrations. This study still needs to be extended to irradiated devices.

8. Conclusions

The electrical behavior of n-in-p and n-in-n pixel sensors has been simulated for different equivalent fluences. Different values have been used for the process parameters. Many guard ring configurations have been used to optimize the protection against breakdown and to keep the depletion region away from the edges, minimizing the dead area at the same time. Even if the simulation is still at a preliminary stage, there is indication that in many layouts it is possible to gain a few hundreds of microns of active area with respect to the present ATLAS sensors, which present a total guard ring plus edge region of about 1.8 mm, thus improving the detector performance.

Simulations indicate that it will be possible to operate the considered detectors even at high fluence without reaching the breakdown voltage, even if the depletion will be only partial.

The capacitance dependence on the geometry, thickness and process parameters has also been studied for unirradiated sensors. The capacitance simulations still need to be extended to irradiated devices.

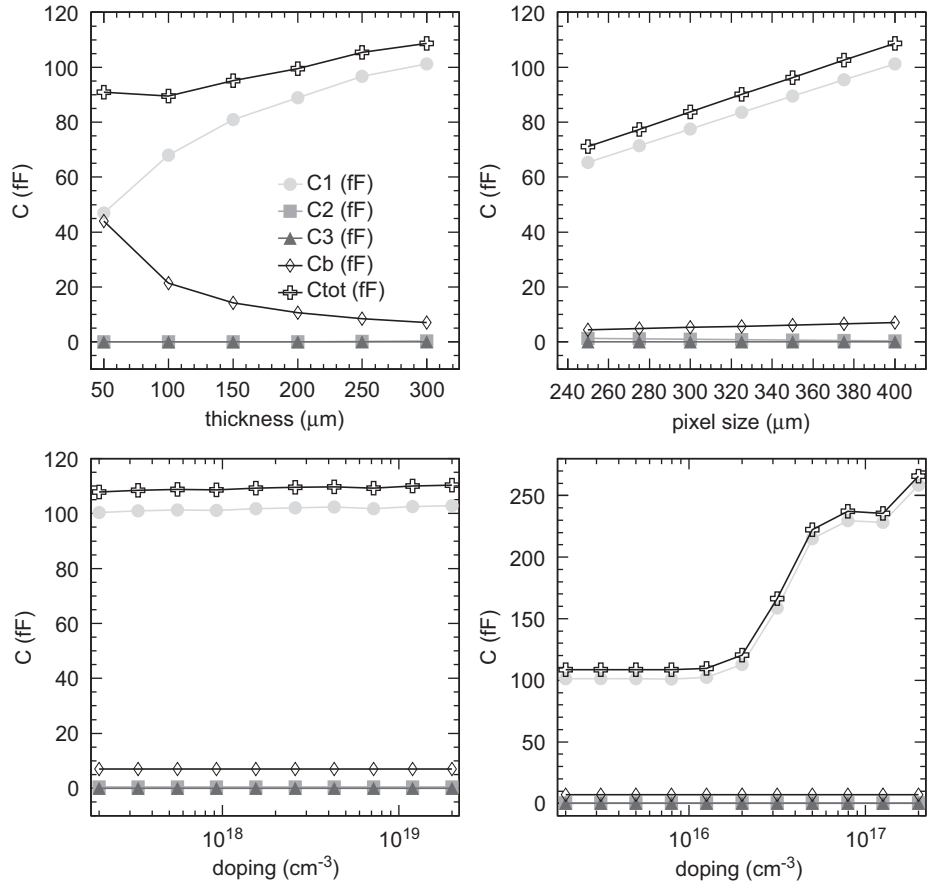

Fig. 7. Different contributions to the pixel capacitance as a function of detector thickness and pixel size (top) pixel doping and p-spray doping concentrations (bottom). C1 is the capacitance towards the first neighbours, C2 versus the second ones, C3 versus the third ones and Cb versus the back.

References

[1] See the official CERN page 〈http://project-slhc.web.cern.ch/project-slhc/about〉.
[2] A. Kok, et al., Nucl. Instr. and Meth. A 560 (2006) 127.
[3] W. Adam, et al., Development of diamond tracking detectors for high luminosity experiments at the LHC, Status Report/RD42, CERN/LHCC 2002-010, 2002.
[4] M. Beimforde, these proceedings.
[5] Silvaco International Inc., 4701 Patrick Henry drive, Bldg. 1, Santa Clara, CA 95054.
[6] W. Shockley, W.T. Read, Phys. Rev. 87 (1952) 835.
[7] C.R. Crowell, S.M. Sze, Appl. Phys. Lett. 9 (1966) 242.
[8] F. Moscatelli, et al., Nucl. Instr. and Meth. B 186 (2002) 171.
[9] Z. Li, H. Kraner, J. Electron. Mater. 21 (1992) 701.
[10] V. Eremin, Z. Li, I. Ilyashenko, Nucl. Instr. and Meth. A 360 (1995) 458.
[11] D. Menichelli, M. Bruzzi, Z. Li, V. Eremin, Nucl. Instr. and Meth. A 426 (1999) 135.
[12] E. Noschis, et al., Nucl. Instr. and Meth. A 574 (2007) 420.
[13] D. Passeri, P. Ciampolini, G. Bilei, F. Moscatelli, IEEE Trans. Nucl. Sci. NS-48 (2001) 1688.
[14] G. Casse, P.P. Allport, A. Greenall, Nucl. Instr. and Meth. A 581 (2007) 318.
[15] G. Casse, A. Affolder, P.P. Allport, IEEE Trans. Nucl. Sci. NS-55 (2008) 1695.